Effects of metal cations on sorption-desorption of *p*-nitrophenol onto wheat ash

Yusheng Wang[1], Zhiguo Pei[1], Xiaoquan Shan[1,*], Guangcai Chen[1,2],
Jing Zhang[3], Yaning Xie[3], Lirong Zheng[3]

1. State Key Laboratory of Environmental Chemistry and Ecotoxicology, Research Center for Eco-Environmental Sciences, Beijing 100085, China.
E-mail: wangyushengly@163.com
2. Research Institute of Subtropical Forestry, Chinese Academy of Forestry, Fuyang 311400, China
3. Synchrotron Radiation Laboratory, Institute of High Energy Physics, Chinese Academy of Sciences, Beijing 100049, China

Abstract

The mutual effects of metal cations (Cu^{2+}, Pb^{2+}, Zn^{2+}, and Cd^{2+}) and *p*-nitrophenol (NP) on their adsorption desorption behavior onto wheat ash were studied. Results suggested that Cu^{2+}, Pb^{2+}, and Zn^{2+} diminished the adsorption and increased the desorption of NP remarkably, while Cd^{2+} had no such effect. In contrast, NP diminished the adsorption of Cu^{2+}, Pb^{2+}, and Zn^{2+} onto ash, however, this suppression effect depended on the initial concentrations of metal cations. NP had no effect on Cd^{2+} adsorption on ash. Fourier transform infrared (FT-IR) and X-ray absorption spectroscopic (XAS) studies suggested the following mechanisms responsible for the metal suppression effect on NP adsorption: (1) large hydrated Cu^{2+}, Pb^{2+}, and Zn^{2+} shells occupied the surface of ash and prevent nonspecific adsorption of NP onto ash surface; (2) Cu^{2+}, Pb^{2+}, and Zn^{2+} may block the micropores of ash, resulting in decreased adsorption of NP; (3) complexation of Cu^{2+}, Pb^{2+}, and Zn^{2+} was likely via carboxyl, hydroxylic and phenolic groups of wheat ash and these same groups may also react with NP during adsorption. As a "soft acid", Cd^{2+} is less efficient in the complexation of oxygen-containing acid groups than Cu^{2+}, Pb^{2+}, and Zn^{2+}. Thus, Cd^{2+} had no effect on the adsorption of NP on wheat ash.

Key words: metal cations; *p*-nitrophenol; adsorption; desorption; wheat ash; FT-IR; XAS

DOI: 10.1016/S1001-0742(10)60381-6

Citation: Wang Y S, Pei Z G, Shan X Q, Chen G C, Zhang J, Xie Y N et al., 2011. Effects of metal cations on sorption-desorption of *p*-nitrophenol onto wheat ash. *Journal of Environmental Sciences*, 23(1): 112–118.

Introduction

Burning of crop residues in the field is a common post-harvest practice for disposal of these materials in many parts of the world. Particulate matter (ashes) resulting from such burning may predominantly contribute to high levels of black carbon (BC) in agricultural soils (Naidu et al., 1998). Ashes can highly adsorb environmental pollutants and strongly influence their fate in the environment (Naidu et al., 1998; Yang and Sheng, 2003). It was also found that crop residue-derived chars appeared to have a higher affinity for polar nitrobenzene than for nonpolar benzene (Chun et al., 2004).

Heavy metals are widely present in the soil environment due to extensive irrigation of agricultural soils with reclaimed wastewater in semiarid and arid areas. Cu, Pb, Zn, and Cd are adsorbed to soil clays via nonspecific and specific adsorption, and have strong affinity for soil organic matter (SOM) (McLean and Bledsoe, 1992). Recently, X ray absorption study revealed that Pb and Cu were predominantly coordinated to carboxylic moieties of peat (Qin et al., 2006; Strawn and Baker, 2008), and form bidentate

inner sphere complexes. When Pb and Cu were adsorbed onto wheat ash (black carbon) complexes were formed through carboxylic, hydroxylic and phenolic groups of ash (Wang et al., 2009).

Nitroaromatic compounds are widely used as pesticides, explosives, and intermediates in the synthesis of dyes, ammunition, and solvents. Nitroaromatics are ubiquitous environmental pollutants. Nitroaromatics and heavy metals often coexist in the environment. The interactions between nitroaromatics and heavy metals tend to govern their fate, and transport behaviors in the environment. However, the effects of metals on the adsorption desorption of nitroaromatics and of nitroaromatics on metal's adsorption onto ash have not been addressed. We selected Cu^{2+}, Pb^{2+}, Zn^{2+}, Cd^{2+} and *p*-nitrophenol (NP) because they occur widely in the environment.

The aim of this study was (1) to explore how Cu^{2+}, Pb^{2+}, Zn^{2+}, and Cd^{2+} affect sorption-desorption behavior of NP on ash and metal, and (2) to provide an insight to the relevant mechanisms responsible for the effects of Cu^{2+}, Pb^{2+}, and Zn^{2+} on the sorption of NP using Fourier transform infrared (FT-IR) and X-ray absorption spectroscopic (XAS) studies.

* Corresponding author. E-mail: xiaoquan@rcees.ac.cn

1 Materials and methods

1.1 Materials

p-Nitrophenol (NP) (purity 97%) was obtained from Beijing Xingjin Company, China, and used without further purification. Its solubility in water is 13,700 mg/L, and its pK_α is 7.15 (Boyd et al., 2001). Pb(NO$_3$)$_2$, Zn(NO$_3$)$_2$, Cu(NO$_3$)$_2$, Cd(NO$_3$)$_2$, Na(NO$_3$)$_2$ and NaN$_3$ were of all guarantee reagent grade. Methanol was of HPLC grade. Wheat ash was obtained by burning wheat straw under natural conditions as described by Yang and Sheng (2003), and was treated in the mixture of hydrochloric acid and hydrofluoric acid (0.1:0.3, mol/L) four times, followed by thorough washing with distilled water to remove soluble salts and silicon.

1.2 Sorption-desorption experiments

All sorption and desorption experiments were performed in triplicates using a batch equilibration method by mixing 20 mg of wheat ash and 25 mL solution of various concentrations of adsorbates which contained 0.01 mol/L NaNO$_3$ as background electrolyte and 0.1 g/L NaN$_3$ as a biocide. The sorption experiments were carried out with either constant concentrations of Cu^{2+}, Pb^{2+}, Zn^{2+}, and Cd^{2+} (0, 0.01, 0.05 or 0.1 mmol/L) containing varying concentrations of NP (20–1200 μg/g) or constant concentration of NP (0, 100, 200, 500 or 1200 μg/g) containing varying concentrations of Cu^{2+}, Pb^{2+}, Zn^{2+}, and Cd^{2+} (0–0.2 mmol/L). We selected pH 4.50 for the adsorption in order to prevent NP from being deprotonated and prevent Pb^{2+}, Zn^{2+}, Cu^{2+} and Cd^{2+} from being hydrolyzed or formation of other unexpected complexes between those metals and NP. Moreover, this pH is consistent with soil pH of red loams in Southern China. The suspensions were shaken for a week (our preliminary test indicated that apparent equilibrium was reached within one week) at 20°C and at pH 4.50 followed by centrifugation at 4000 ×*g* for 20 min. Then the concentrations of NP and Cu^{2+}, Pb^{2+}, Zn^{2+}, and Cd^{2+} in the supernatants were determined by high pressure liquid chromatography (HPLC) and inductively coupled plasma-optical emission spectrometry (ICP-OES, Perkin-Elmer, USA), respectively.

The desorption background solution containing 0.01 mol/L NaNO$_3$ and 0.1 g/L NaN$_3$ was previously equilibrated with ash for the same time as for the adsorption experiments of NP. Desorption experiments of NP were conducted in sequential decant-refill steps immediately following completion of sorption experiments with one weak. At the end of adsorption experiments, 15 mL aliquot of centrifuged supernatant was withdrawn and refilled with the same volume of desorption background solution in the absence and presence of metals. The concentrations of the metals in the supernatant after the adsorption were used in the desorption solution. The tubes were shaken for additional one week and then centrifuged again. The above process was repeated three cycles. The NP concentration present in the supernatant after each desorption cycle was determined by HPLC analysis. Desorbed NP was calculated at each desorption stage.

1.3 Analysis

The concentrations of NP was determined by Hewlett-Packard Model 1100 gradient HPLC system (Agilent Technologies, USA) equipped with an autoinjector, photodiode-array UV-Visible detector at 254 nm, and an extended polar selectivity reversed-phase column (15 cm × 4.6 mm i.d.). The mobile phase was a mixture of methanol and water (60:40, *V/V*) with a flow rate of 0.7 mL/min. The concentrations of Cu^{2+}, Pb^{2+}, Zn^{2+}, and Cd^{2+} were determined by ICP-OES.

1.4 Characterization

Wheat ash was subjected to crossed polarization magic angle spinning nuclear magnetic resonance (CPMAS ^{13}C NMR) analysis by a Bruker Advance 300 MHz NMR spectrometer (Varian, USA) to obtain its chemical group distribution. Spectra were acquired at a frequency of 75 MHz with a ^{13}C MAS spinning rate of 13 kHz, contact time of 2 msec, 1 sec recycle delay. The number of scans ranged from 5000 to 10,000 per sample. Scanning Electron Microscopy (S-3000N, Hitachi, Japan) was used to obtain its surface feature. Nitrogen specific surface area (SSA) of wheat ash was measured using Brunauere-Emmett-Teller (BET) equation for sorption of N$_2$ at 77 K. The samples of wheat ash, NP, NP adsorbed ash, Zn^{2+} adsorbed ash and their supernatant samples was applied for attenuated total reflection Fourier transform infrared (ATR-FT-IR) spectra (GX2000 FT-IR spectrometer, Perkin-Elmer, USA) (Pei et al., 2010). Briefly, after sorption and centrifugation, the paste and supernatant were collected separately, and immediately spread on ZnSe crystal surface to obtain an appropriate thin layer. The sample holding region was sealed with a lid to prevent evaporation, and the FT-IR spectra were measured. The resolution of the FT-IR spectra was 2.0 cm^{-1}, and a total of 64 scans were collected for each spectrum. FT-IR spectra of ash in 0.01 mol/L NaNO$_3$ were also measured in the absence of NP and/or metals. For aqueous NP, difference spectra were obtained by subtracting the background electrolyte solution spectra from the spectra of the NP solution. For ash alone, NP or metal adsorbed ash, the difference spectra were obtained by subtracting their corresponding supernatant from the spectra of ash alone, NP or metal adsorbed ash. The XANES (X-ray adsorption near-edge structure) and EXAFS (extended X-ray adsorption fine structure) spectra of the Cu, Pb, Zn absorbed ash and reference compounds were collected at the Beijing Synchrotron Radiation Facility (BSRF). The experimental details were described previously (Wang et al., 2009).

1.5 Data analysis

Sorption-desorption data were fitted to the Freundlich equation:

$$q_e = K_F C_e^N$$

where, K_F ((mg/g)/(μg/g)^N) is Freundlich affinity coefficient, N is Freundlich exponential coefficient, q_e (μg/g) is the amount of NP sorbed by wheat ash, and C_e is (μg/g)

is the equilibrium concentration in solution. OMNIC 6.0 and WinXAS 2.1 were used for FT-IR and EXAFS data analyses, respectively. Statistical analyses were performed using Origin 7.0 and SPSS 11.5.

2 Results and discussion

2.1 Ash characteristics

The ^{13}C NMR spectra of wheat ash are presented in Fig. 1. A dominant peak of ash was observed at 130 ppm, which can be assigned primarily to aromatic structures, consistent with NMR spectra of crop derived chars (Chun et al., 2004). Wheat ash has low aliphatic C (0–110 ppm) content of 15.8%, high aromatic C (110–145 ppm) content of 73%, low phenolic C (145–163 ppm) content of 9.0%, and low carboxyl C (163–190 ppm) content of 2.6%. Those NMR results were in agreement with the elemental analysis (see discussion below).

Wheat ash has large BET surface area, sorptive capability, and percentage of aromatic carbon, high organic carbon (OC) and low H and O contents, which are similar to those reported for wood-made chars and wheat ash (Yang and Sheng, 2003; Chun et al., 2004), indicating high carbonization of wheat ash. Wheat ash has large BET surface area of 410.7 m^2/g, reflecting the ash's fine-pore structures.

Wheat ash has H/C, O/C and (N+O)/C atomic ratios of 0.40, 0.18 and 0.19, respectively, which are similar with 0.51–0.73, 0.11–0.24, and 0.12–0.23 of black carbon isolated from soil and sediments, and are comparable to those of typical charcoal derived from coals as well (Song et al., 2002). The H/C, O/C and (N+O)/C atomic ratios of wheat ash are also consistent with those of the wood chars treated under oxygen limited conditions (Chun et al., 2004; Wang et al., 2006), but higher than those of activated carbon. The findings suggested that the low temperature burned wheat ash was more polar in keeping with their water uptake because of partial carbonization. Since H is mainly associated with plant OC (Kuhlbusch, 1995), degree of carbonization can be characterized by

atomic ratio of H/C because polar groups of ashes usually work as water binding centers and facilitate formation of water clusters (Bandosz et al., 1993). H/C ratio 0.40 of wheat ash indicated there was a good amount of plant organic residues in wheat ash. (N+O)/C or O/C ratio is an indicative of polarity and hydrophobicity. Low (N+O)/C or O/C ratio suggested low polar groups content in wheat ash, reflecting the mitigation of its hydrophilicity, and consequently reduced affinity for water molecules.

2.2 Effect of pH on the adsorption of NP

The adsorption of NP onto ash remained constant over low pH range of 2.0–6.0, but decreased dramatically with increasing pH from 6.0 to 9.0 (data not shown). As a weak acid with pKa of 7.15, NP was present mainly as neutral molecules over pH 2.0–6.0 and thus the adsorption of NP to ash was unchanged. When pH was further increased NP was deprotonated, thus the adsorbed NP decreased due to the lower hydrophobicity of deprotonated NP, as well as the repulsive forces between the negatively charged surface of ash and deprotonated NP.

2.3 Competitive sorption of heavy metals and NP

The adsorption isotherms of NP in the presence of Cu^{2+}, Pb^{2+}, and Zn^{2+} were nonlinear (Fig. 2). Freundlich model was found to fit the sorption isotherms well. The presence of 0.1 mmol/L Cu^{2+}, Pb^{2+} and Zn^{2+} decreased the adsorption of NP at its initial concentration of 200 mg/L by 16%, 25%, and 20%, respectively. However, the suppressive effects were metal concentration-dependent (Fig. 2). It should be pointed out that Cd^{2+} had little effect on the adsorption of NP (data not shown) because Cd^{2+} is a "soft" acid (Tamara et al., 2007), and thus Cd^{2+} is less efficient in complexing oxygen containing groups of ash than Cu^{2+}, Pb^{2+}, and Zn^{2+}.

The adsorption of Cu^{2+}, Pb^{2+}, Zn^{2+}, and Cd^{2+} in the absence and presence of NP was also studied and NP tends to diminish the adsorption of Cu^{2+}, Pb^{2+}, and Zn^{2+} onto ash. This suppression effect depended on the initial concentrations of metal cations. The presence of 200 mg/L NP decreased the adsorption of 0.2 μg/g Cu^{2+}, Pb^{2+}, and Zn^{2+} by 22%, 16%, and 14%, respectively. As expected that NP had no effect on Cd^{2+} adsorption onto ash. This provides an evidence for direct competitive adsorption between NP and the hydrated Cu^{2+}, Pb^{2+}, and Zn^{2+} cations.

2.4 Effects of Pb^{2+}, Zn^{2+}, and Cu^{2+} on the desorption of NP

Sorption and desorption isotherms were compared to assess desorption hysteresis. Due to short equilibrium time of 24 hr was employed, it is not appropriate to refer to discrepancy between the sorption and desorption flanks of the isotherms as true hysteresis because sorption reaction may have continued beyond the point in time when desorption experiment was initiated. Desorption of NP was found to be hysteretic. The ratio of Freundlich exponents of desorption (N_d) to sorption (N_s), N_d/N_s, was defined as desorption hysteresis index (HI) (Table 1). Desorption hysteresis coefficient of 1 means no desorp-
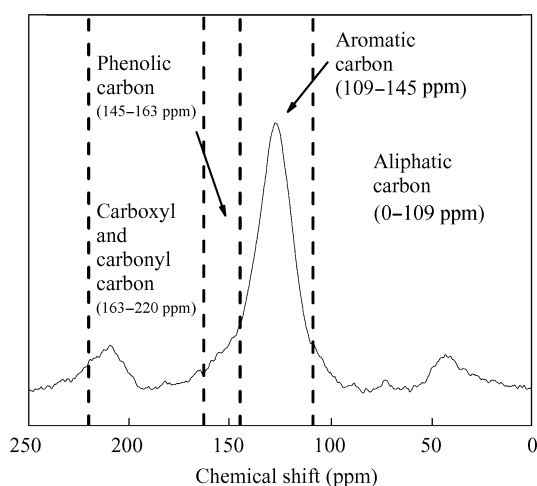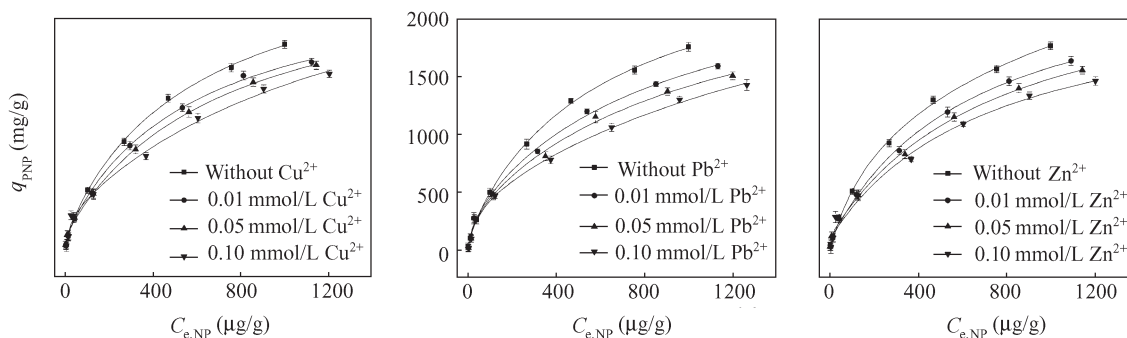

Fig. 1 ^{13}C NMR spectra of ash.

Fig. 2　Effects of Cu^{2+}, Pb^{2+}, and Zn^{2+} on the adsorption of NP onto ash.

Table 1　Freundlich constants and hysteresis indexes of NP sorption from ash in the absence and presence of metals

In the absence of M^{2+} $K_F = 40.50 \pm 1.27$ $N_s = 0.551 \pm 0.012$			In the presence of Pb^{2+} $K_F = 35.37 \pm 0.59$ $N_s = 0.514 \pm 0.012$			In the presence of Zn^{2+} $K_F = 36.10 \pm 0.67$ $N_s = 0.519 \pm 0.010$			In the presence of Cu^{2+} $K_F = 36.94 \pm 0.49$ $N_s = 0.526 \pm 0.013$		
N_d	HI	R^2	N_d	HI	R^2	N_d	HI	R^2	N_d	HI	R^2
0.051	0.093	0.99	0.050	0.097	0.92	0.052	0.100	0.95	0.052	0.099	0.98
0.087	0.158	0.99	0.113	0.220	0.99	0.099	0.191	0.97	0.093	0.177	0.93
0.136	0.247	0.98	0.147	0.286	0.95	0.130	0.250	0.93	0.117	0.222	0.95
0.160	0.291	0.95	0.177	0.344	0.98	0.168	0.324	0.98	0.163	0.310	0.97
0.185	0.336	0.96	0.207	0.403	0.98	0.195	0.376	0.99	0.178	0.338	0.94
0.080	0.145	0.93	0.152	0.296	0.96	0.151	0.291	0.98	0.153	0.291	0.99

tion hysteresis of NP from wheat ash. The smaller HI corresponds to the greater degree of hysteresis (Yuan and Xing, 2001). In all cases desorption of NP was hysteretic. Desorption increased from low to high initial equilibrium concentrations of NP and then decreased at the highest NP concentration as shown in N_d values. This trend can be explained by the limited number of sites available for high energy binding. At low equilibrium concentrations of NP, NP molecules bind to high energy sites, resulting in smaller N_d values. At higher concentrations of NP, more NP molecules occupy low energy sites which can be more readily desorbed, and thus a larger desorption N_d was obtained. At the highest concentrations of NP, NP molecules caused structural swelling of ash, which led to additional binding sites becoming available and reduced desorption N_d again.
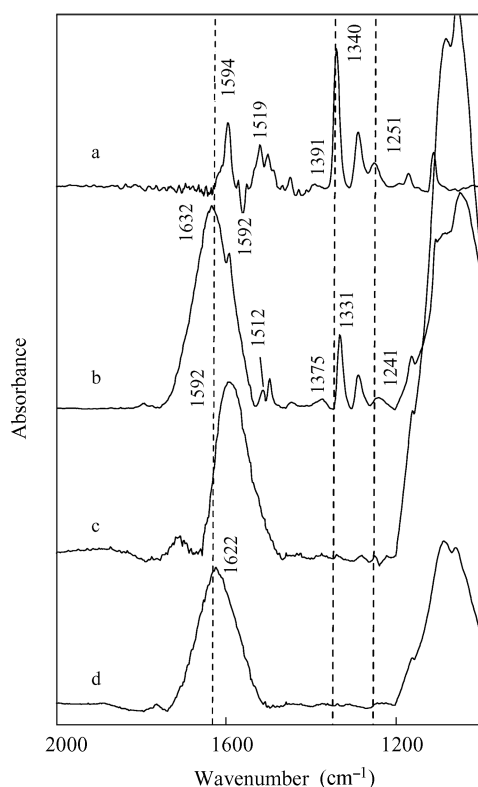
When no metal was present the HI indexes were in the range of 0.093–0.145 for equilibrium concentrations of 20–1200 μg/g NP, whereas the HI indexes were in the range of 0.097–0.246, 0.100–0.150 and 0.099–0.293 for NP in the presence of 0.1 mmol/L Pb^{2+}, Zn^{2+}, and Cu^{2+}, respectively, indicating Cu^{2+}, Pb^{2+}, and Zn^{2+} binding to high energy sites rendered NP adsorption onto low energy sites, and thus making NP desorption relatively easy.

2.5 Spectroscopic evidence for the suppression effects of metal cations on NP sorption

Johnston et al. (2002) comprehensively studied the sorption of 4,6-dinitro-*o*-cresol (DNOC) to smectite using FT-IR, HPLC, and quantum chemical methods and verified that electron donor-acceptor (EDA) interaction was not operative. The result indicates that π-π EDA mechanism

is not responsible for the adsorption of NP because NP is considered a weaker acceptor. Therefore, we excluded π-π EDA mechanism as a mechanism responsible for the adsorption of NP onto ash, and assumed that several other mechanisms are mainly responsible for the observed suppression effects of Cu^{2+}, Pb^{2+}, and Zn^{2+} on the sorption of NP. First, large hydrated Cu^{2+}, Pb^{2+}, and Zn^{2+} shells occupy the surface of ash and prevent nonspecific adsorption of NP onto ash surface. This assumption was strongly supported by Chen et al. (2008), who studied the adsorption of hydrophobic organic compounds to wood charcoal as affected by heavy metals. Second, hydrated Cu^{2+}, Pb^{2+}, and Zn^{2+} occupy or block micropores of ash. Our previous work indicated that the micropore structure size of ash (0.25–1.5 nm accounts for 65.6% of cumulative micropore and mesopore volumes) matches the size of hydrated metal ions well (0.4–0.5 nm of hydrated Cu^{2+}) (Wang et al., 2009). The molecular size of NP is calculated to be 0.66 nm × 0.43 nm (Huang et al., 2009). In this case competition takes place in the hole-filling domain. Third, competitive adsorption occur between Cu^{2+}, Pb^{2+}, Zn^{2+} and NP for the same adsorption sites of oxygen containing groups such as carboxylic, carbonyl and hydroxyl groups.

To reveal the sorption sites of NP on ash, an ATR-FT-IR study was performed. Because FT-IR study of Pb and Cu has been reported previously (Wang et al., 2009), Fig. 3 shows the FT-IR spectra of NP, NP adsorbed ash, ash, and Zn^{2+} adsorbed ash in the frequency range of 1000–2000 cm^{-1}. FT-IR spectra of NP alone (Fig. 3a) contained peaks attributable to asymmetric and symmetric (υ_{NO}) stretching vibrations (1519 and 1340 cm^{-1}), phenolic –OH deformation vibration (1391 cm^{-1}), and C–O stretching

Fig. 3 FT-IR spectra of NP alone (line a), NP adsorbed ash (line b), ash (line c), and Zn^{2+} adsorbed ash (line d).

Table 2 XAFS results of Zn adsorbed ash and Zn reference compounds

	Neighboring atoms	R (Å)[a]	CN[b]	$\Delta\sigma^2$ (Å²)[c]
$Zn(CH_3COO)_2$	Zn–O	0.196	4.26	0.008
Zn^{2+}(aq)	Zn–O	0.208	5.79	0.010
$Zn(OH)_2$	Zn–O	0.195	3.82	0.009
Zn^{2+} adsorbed-ash	Zn–O	0.200	4.68	0.010

[a] Interatomic distance, [b] coordination number, [c] Debye-Waller factor (Å²).

Two different inflections at 9.660 and 9.664 eV of first derivative spectra (Fig. 4b) represented degree of axial distortion and covalence of equatorial ligands bonded to Zn^{2+} ions. Spectrum position at 9.664 eV was very close to those of four coordinated Zn bearing compounds such as ZnO, and Zn acetate, suggesting an oxidation state of +2 and tetrahedral environment in ash. The decreased peak intensity of Zn-adsorbed ash than that of $Zn(NO_3)_2$ was influenced by degree of bond covalency and local structural disorder, and thus indicated that stronger field water molecules in the tetragonal plane associated with Zn^{2+} were partly replaced by weak field organic groups (e.g., carboxylic group) of ash. k^3-weighted EXAFS spectra and their corresponding radial structural function (RSF) derived from Fourier transformation of the samples are presented in Fig. 4c, d. The strongest peak occurring at 0.178 nm (Fig. 4d) corresponded to first-shell O atoms. Analyses of the XANES and EXAFS results of Zn adsorbed-ash, and their reference compounds suggested that the coordination environment of Zn adsorbed ash strongly resembles that of $Zn(CH_3COO_2)_2$. Zn was coordinated with 4.68 oxygen atoms through carboxylic, phenolic and hydroxylic groups. The bond length was found to be 0.200 nm, which was shorter than that of hydrated Zn^{2+} in aqueous solution (0.208 nm) and longer than that of $Zn(CH_3COO_2)_2$. The above XANES and EXAFS results were supported by Pokrovsky et al. (2005), who studied speciation of Zn in diatoms and results indicated that Zn was surrounding by (4.0 ± 0.5) oxygens in the first coordination shell with average Zn–O distances of (0.200 ± 0.002) nm for adsorbed Zn and (0.197 ± 0.002) nm for incorporated inside the cell. The above XANES and EXAFS study suggested that Zn may form inner-sphere complexes via carboxylic, phenolic and hydroxylic groups of ash when Zn was adsorbed onto ash.

3 Conclusions

An integrated method of macro- with micro-spectroscopic studies revealed the underlying mechanisms responsible for mutual effects of metal cations (Cu^{2+}, Pb^{2+}, Zn^{2+}) and NP on their adsorption on and/or desorption from wheat ash, implying that the environmental fate of metal cations and NP in the metal-NP system is quite different from that of either metals or NP alone. Such information helps understand the real environmental processes of metals and aromatics in the soil environment.

vibration (1251 cm^{-1}). When NP was adsorbed on ash, it was found that the asymmetry and symmetry stretching of N–O group of NP at 1519 cm^{-1} and 1340 cm^{-1} (Fig. 3a) shifted to 1512 cm^{-1} and 1331 cm^{-1} (Fig. 3b), simultaneously, the phenolic –OH deformation vibration at 1391 cm^{-1} (Fig. 3a) and the C–O stretching vibration at 1251 cm^{-1} shifted to 1375 and 1241 cm^{-1}, respectively (Fig. 3b). It is obvious that both phenolic –OH and –NO$_2$ were simultaneously involved in the sorption of NP (Saltzman and Yariv, 1975). Figure 3c is FT-IR spectra of ash, in which the broad band at 1592 cm^{-1} may be attributed to the stretching vibration of C=O band of phenyl ring on ash (Wang et al., 2009). After NP was adsorbed onto ash, this band was shifted to 1632 cm^{-1}, which indicated that C=O group on phenyl ring of wheat ash participated in reaction with phenolic –OH and –NO$_2$ of NP. Similarly, when Zn^{2+} was adsorbed the stretching vibration of C=O band of ash shifted from 1592 to 1622 cm^{-1} (Fig. 3d). It seemed that these groups on ash were responsible for the adsorption of Zn^{2+}, which would be further verified in the following XAFS section.

Complexation of Cu and Pb via carboxylic, hydroxylic and phenolic groups of ash has been discussed previously (Wang et al., 2009). Our efforts are only to provide an insight to the participation of carboxylic, hydroxylic and phenolic groups of ash responsible for the adsorption of Zn on ash in this study. XANES and EXAFS spectra of zinc adsorbed ash, and zinc reference compounds are shown in Fig. 4, and XAS parameters are shown in Table 2.

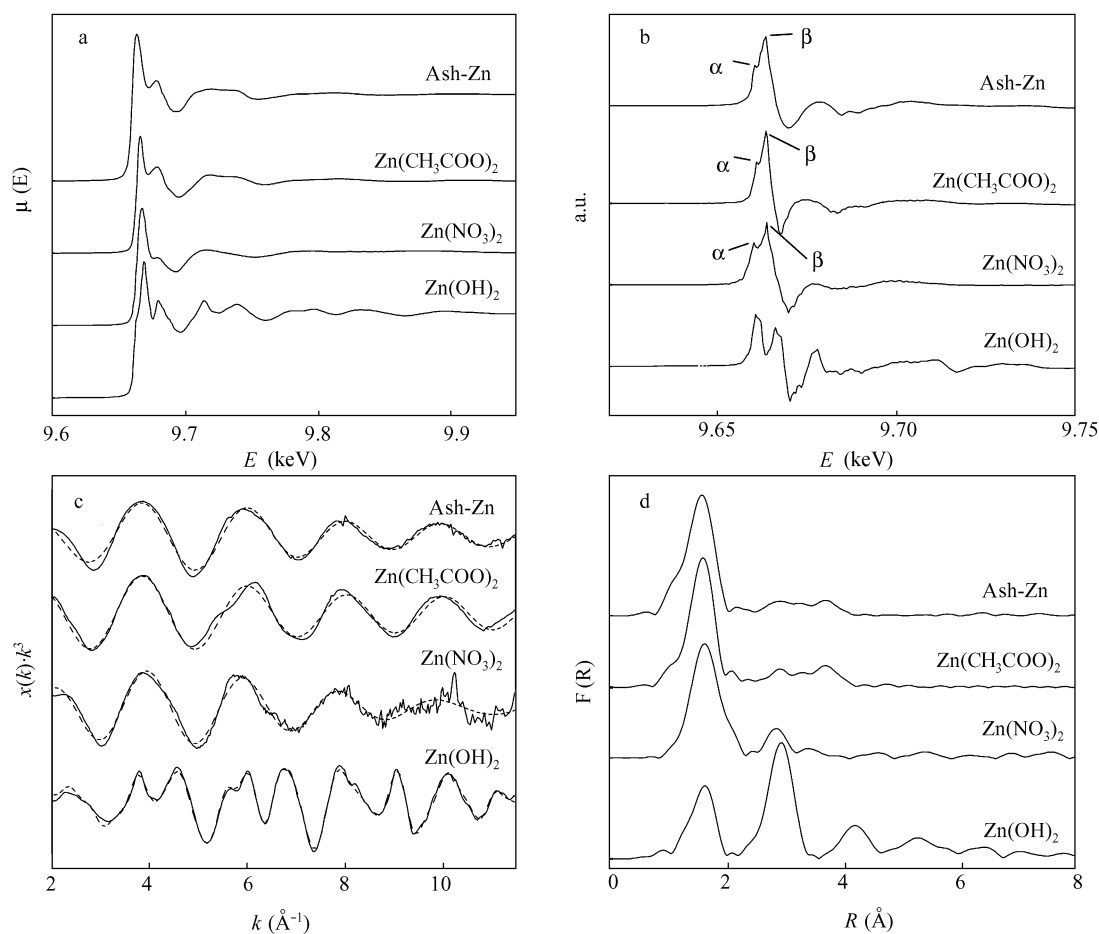**Fig. 4** XAS spectra of Zn adsorbed ash and Zn reference compounds. (a) normalized XANES spectra; (b) first derivatives; (c) raw and fitted EXAFS spectra (χ-function); (d) Fourier transformation of EXAFS spectra.

References

Bandosz T J, Jagiello J, Schwarz J A, 1993. Effect of surface chemical groups on energetic heterogeneity of activated carbons. *Langmuir*, 9: 2518–2522.

Boyd S A, Sheng G, Teppen B J, Johnston C T, 2001. Mechanisms for the adsorpiton of substituted nitrobenzenes by smectite clays. *Environmental Science & Technology*, 35: 4227–4234.

Chen G C, Shan X Q, Wang Y S, Pei Z G, Shen X E, Wen B et al., 2008. Effects of copper, lead, and cadmium on the sorption and desorption of atrazine onto and from carbon nanotubes. *Environmental Science & Technology*, 42: 8297–8302.

Chun Y, Sheng G Y, Chiou C T, Xing B, 2004. Compositions and sorptive properties of crop residue-derived chars. *Environmental Science & Technology*, 38: 4649–4655.

Huang J H, Yan C, Huang K L, 2009. Removal of *p*-nitrophenol by a water-compatible hypercrosslinked resin functionalized with formaldehyde carbonyl groups and XAD-4 in aqueous solution: A comparative study. *Journal of Colloid and Interface Science*, 332: 60–64.

Johnston C T, Sheng G, Teppen B J, Boyd S A, De Oliveira M F, 2002. Spectroscopic study of dinitrophenol herbicide sorption on smectite. *Environmental Science & Technology*, 36: 5067–5074.

Kuhlbusch T A J, 1995. Method for determining black carbon in residues of vegetation fires. *Environmental Science & Technology*, 29: 2695–2702.

McLean J E, Bledsoe B E, 1992, "Behavior of Metals in Soils" in "Ground Water Issue". United States Environmental Protection Agency, EPA/540/S-92/018.

Naidu R, Sumner M E, Harter R D, 1998. Adsorption of heavy metals in strongly weathered soils, an overview. *Environmental Geochemistry and Health*, 20: 5–9.

Pei Z G, Shan X Q, Kong J J, Wen B, Owens G, 2010. Coadsorption of ciprofloxacin and Cu(II) on montmorillonite and kaolinite as affected by solution pH. *Environmental Science & Technology*, 44: 915–920.

Pokrovsky O S, Pokrobski G S, Gelabert A, Schott J, Boudou A, 2005. Speciation of Zn associated with diatoms using X-ray absorption spectroscopy. *Environmental Science & Technology*, 39: 4490–4498.

Qin F, Wen B, Shan X Q, Xie Y N, Liu T, Zhang S Z et al., 2006. Mechanisms of competitive adsorption of Pb, Cu, and Cd on peat. *Environmental Pollution*, 144: 669–680.

Saltzman S, Yariv S, 1975. Infrared study of the sorption of phenol and *p*-nitrophenol by montmorillonite. *Soil Science Society of America Journal*, 39: 474–479.

Song J Z, Peng P A, Huang W L, 2002. Black carbon and kerogen in soils and sediments. 1. Quantification and characteriza-

tion. *Environmental Science & Technology*, 36: 3960–3967.

Strawn D G, Baker L L, 2008. Speciation of Cu in a contaminated agricultural soil measured by XAFS, μ-XAFS, and μ-XRF. *Environmental Science & Technology*, 42: 37–42.

Tamara P S, Michal N, Benny C, 2007. Binding of pyrene to hydrophobic fractions of dissolved organic matter: effect of polyvalent metal complexation. *Environmental Science & Technology*, 41: 5389–5394.

Wang X L, Sato T, Xing B S, 2006. Competitive sorption of pyrene on wood chars. *Environmental Science & Technology*, 40: 3267–3272.

Wang Y S, Feng M H, Shan X Q, Chen G C, Pei Z G, Wen B et al., 2009. Effects of copper, lead, and cadmium on the sorption of 2,4,6-trichlorophenol onto and desorption from wheat ash and two commercial humic acids. *Environmental Science & Technology*, 43: 5726–5731.

Yang Y N, Sheng G Y, 2003. Enhanced pesticide sorption by soils containing particulate matter from crop residue burns. *Environmental Science & Technology*, 37: 3635–3639.

Yuan G S, Xing B S, 2001. Effects of metal cations on sorption and desorption of organic compounds in humic acids. *Soil Science*, 166: 107–115.